Journal of Molecular Structure 1220 (2020) 128642

Contents lists available at ScienceDirect

Journal of Molecular Structure

journal homepage: http://www.elsevier.com/locate/molstruc

Nanochanneled silver-deficient tris(oxalato)chromate(III) coordination polymers: Synthesis, crystal structure, spectroscopy, thermal analysis and magnetism

Augustin N. Nana [a], Delia Haynes [b], Hervé Vezin [c], Claire Minaud [d], Pritam Shankhari [e], Boniface P.T. Fokwa [e, **], Justin Nenwa [a, *]

[a] Inorganic Chemistry Department, University of Yaounde 1, P.O. Box 812, Yaounde, Cameroon
[b] Department of Chemistry and Polymer Science, Stellenbosch University, P. Bag X1, Matieland, 7602, South Africa
[c] Université de Lille, LASIRE CNRS UMR 8516, 59655, Villeneuve d'Ascq, Lille, France
[d] Université de Lille, Institut Chevreul CNRS FR2638, 59655, Villeneuve d'Ascq, Lille, France
[e] Chemistry Department, University of California Riverside, 501 Big Springs Rd, Riverside, CA, 92521, USA

ARTICLE INFO

Article history:
Received 31 March 2020
Received in revised form
1 June 2020
Accepted 6 June 2020
Available online 16 June 2020

Keywords:
Silver-deficient salts
Tris(oxalato)chromate(III) complexes
Coordination polymers
Nanochannels
Magnetic properties

ABSTRACT

Two silver-deficient tris(oxalato)chromate(III) coordination polymers, $SrK_{0.5}Ag_{0.5}[Cr(C_2O_4)_3]$ (**1**) and $SrAg[Cr(C_2O_4)_3]\cdot 6H_2O$ (**2**) have been synthesized and fully characterized by elemental and TGA-DSC analyses, IR and UV–Vis spectroscopies, single-crystal X-ray diffraction and magnetic measurements. Salt **1** crystallizes in the orthorhombic polar space group *Fdd2*, whereas **2** crystallizes in the monoclinic space group $P2_1/c$. Compared to the well-known salt $Ag_3[Cr(C_2O_4)_3]\cdot 3H_2O$ with no silver deficiency, **1** and **2** can be seen as nanochanneled silver-deficient oxalatochromate(III) coordination polymers featuring silver deficiency values of 2.5 and 2.0, respectively. In **1**, nanochannels host K^+ and Ag^+ cations, whereas in **2**, they solely host hydrogen-bonded water molecules. The magnetic properties of **1** and **2** have been investigated in the temperature range 2–300 K. The decrease of $\chi_M T$ observed at low temperatures for 1 and **2** revealed weak antiferromagnetic interactions in the two compounds.

1. Introduction

Coordination polymers (CPs), pioneered by Robson, Kitagawa and Yaghi groups [1–4] represent a new class of crystalline materials obtained by the assembly of organic and/or inorganic ligands and metal ions. These CPs have gained increasing attention over the past few decades due to their fascinating structures and great potential applications in catalysis [5,6], magnetism [7,8], non-linear optics [9,10], gas storage and separation processes [11–13]. Recently, Constable introduced a *Research Front on silver CPs* [14] as an attractive area of study within the field of crystal engineering. He laid emphasis on the versatility of silver-containing CPs in respect of their many key features such as variable coordination numbers and geometries, differing modes of metal-ligand linkages, silver-silver interactions, photophysical, electronic, and biomedical applications.

Dean et al. have described a family of CPs with a variable Ag–Cr-oxalate channel structures, formulated as $[(M_xAg_{0.50-x})(H_2O)_3]@[Ag_{2.50}Cr(C_2O_4)_3]$ ($0 \leq x \leq 0.50$; M = K, Cs, Ag) [15]. These silver salts generally crystallize in a nonmolecular polymer framework with flexible deficiencies x of Ag^+ ions. They thus generate negatively charged frameworks with chemical compositions $[Ag_{3-x}Cr(C_2O_4)_3]^{x-}$, where the negative charge (−x) is offset by an equivalent charge from protons [16,17], cations (M^+) from group 1 elements [15,18], cations (M^{2+}) from group 2 elements [19] or from metal(III) ions [20]. These CPs share in their crystal structures the one-dimensional channel lattice as one of their characteristic features.

To date, authors have investigated mainly the structural aspects of these silver-deficient tris(oxalato)chromate(III) CPs, and very little attention has been paid to their magnetic properties so far [15–20]. For these reasons, in this paper, we aimed to widen the scope of this family of nanochanneled CPs, a special emphasis being set on the increase of silver deficiency x of the negatively charged lattice framework $[Ag_{3-x}Cr(C_2O_4)_3]^{x-}$ and on the study of magnetic

* Corresponding author.
** Corresponding author.
E-mail addresses: bfokwa@ucr.edu (B.P.T. Fokwa), jnenwa@yahoo.fr (J. Nenwa).

https://doi.org/10.1016/j.molstruc.2020.128642
0022-2860/

properties of the resulting structures. Herein, we report two new members of this family of CPs, namely $SrK_{0.5}Ag_{0.5}[Cr(C_2O_4)_3]$ (**1**) and $SrAg[Cr(C_2O_4)_3]\cdot 6H_2O$ (**2**), with silver deficiency values of 2.5 and 2.0 per formula unit, respectively. These silver deficiency values are the highest obtained so far for this family of salts. The thermal stability as well as the magnetic properties of the two salts have been examined in detail.

2. Experimental

2.1. Materials and measurements

All the chemicals were commercially available and used as received. The precursor salt $Ag_3[Cr(C_2O_4)_3]\cdot 3H_2O$ was prepared according to the literature procedure [15]. All the reactions were carried out in distilled water. Elemental analyses (C and H) were performed on a Fisons-EA 1108 CHN elementar analyzer. IR spectra (4000−400 cm^{-1}) were recorded using a PerkinElmer 2000 FT−IR spectrometer with KBr used as medium. UV/Vis spectra were performed with a Bruker HACH DR 3900 spectrophometer, in water, in the range 300−800 nm. Thermogravimetric analysis (TGA) and differential scanning calorimetry (DSC) were carried out using a LINSEIS STA PT-1000 thermal analyzer. The powdered sample (20 mg) was heated from 25 to 700 °C with a rate of 10 °C/min in flowing air. Powder X-ray diffraction PXRD data for **1** were collected using a Bruker D2 Phaser benchtop powder diffractometer equipped with a copper source (1.54183 Å radiation). Data were collected from $2\theta = 4–50°$. PXRD data for **2** were recorded with a Bruker D8Advance diffractometer at 40 kV and 40 mA for a Cu-target tube ($\lambda = 1.54056$ Å). EPR spectra were collected using a Bruker ELEXYS E500 operating at 9 GHz. The spectra were recorded at room temperature with a microwave power of 0.3 mW and an amplitude modulation of 3G. A Quantum Design MPMS-5XL SQUID magnetometer was used to collect magnetic susceptibility data. Measurements were done at 0.1 T down to 2 K on polycrystalline samples. Diamagnetic corrections were made with Pascal's constants for all the constituent atoms as well as the contributions of samples holder [21].

2.2. Syntheses

2.2.1. Synthesis of $SrK_{0,5}Ag_{0,5}[Cr(C_2O_4)_3]$ (**1**)

A mixture of $Ag_3[Cr(C_2O_4)_3]\cdot 3H_2O$ (0.69 g, 1 mmol), $SrCl_2\cdot 6H_2O$ (0.14 g, 1 mmol), KCl (0.04 g, 0.5 mmol) and water (50 mL) was stirred at 60 °C for 2 h in air under ambient conditions. The reaction mixture was gradually cooled to 25 °C and filtered. The purple filtrate was allowed to evaporate in a hood at room temperature. Purplish block-shaped crystals suitable for X-ray diffraction were collected after three months. Yield: 430 mg (0.90 mmol, 83%) based on KCl. Anal. calcd (%) for **1**: C, 15.02. Found (%): C, 14.98. IR data (cm^{-1}): 1636 (s), 1416 (s), 1275 (m), 853 (s), 543 (s), 474 (s), 409 (s) (Fig. S1). UV−Vis (H_2O solution, nm): 418, 569 (Fig. S3).

2.2.2. Synthesis of $SrAg[Cr(C_2O_4)_3]\cdot 6H_2O$ (**2**)

A mixture of $Ag_3[Cr(C_2O_4)_3]\cdot 3H_2O$ (0.69 g, 1 mmol), $SrCl_2\cdot 6H_2O$ (0.14 g, 1 mmol) and water (50 mL) was stirred at 60 °C for 2 h in air under ambient conditions. The reaction mixture was gradually cooled to 25 °C and filtered. The purple filtrate was allowed to evaporate in a hood at room temperature. Purplish block-shaped crystals suitable for X-ray diffraction were harvested after two months. Yield: 510 mg (0.82 mmol, 82%) based on $SrCl_2\cdot 6H_2O$. Anal. calcd (%) for **2**: C, 11.62; H, 1.93. Found (%): C, 11.55; H, 1.95. IR data (cm^{-1}): 3407 (w), 1626 (s), 1380 (s), 1255 (m), 543 (s), 476 (s), 409 (s) (Fig. S2). UV−Vis (H_2O solution, nm): 420, 571 (Fig. S4).

2.3. Crystal structure determination

Single crystal X-ray diffraction data for **1** and **2** were recorded with a Bruker Smart Apex II diffractometer with graphite-monochromated Mo-$K\alpha$ radiation ($\lambda = 0.71073$ Å) at 293 K.

Table 1
Crystal data and structure refinements for **1** and **2**.

Compound	1	2
Empirical formula	$C_6Ag_{0.50}CrK_{0.50}O_{12}Sr$	$C_6H_{12}AgCrO_{18}Sr$
Formula weight	479.39	619.65
T (K)	293(2)	293(2)
λ (Å)	0.71073	0.71073
Crystal system	Orthorhombic	Monoclinic
Space group	*Fdd2*	$P2_1/c$
Unit Cell parameters a (Å)		
a (Å)	36.092(3)	8.3584(5)
b (Å)	14.225(2)	11.0370(7)
c (Å)	11.0832(10)	19.2301(10)
α (°)	90	90
β (°)	90	91.285(5)
γ (°)	90	90
V ($Å^3$)	5690.2(11)	1773.56(18)
Z	16	4
μ (mm^{-1})	5.383	4.782
F(0 0 0)	3622	1204
Crystal size (mm)	0.09 × 0.10 x 0.17	0.18 × 0.30 x 0.30
θ range for data collection (°)	2.880−33.679	2.810−33.526
Index ranges	$-55 \le h \le 13, -15 \le k \le 21, -16 \le l \le 12$	$-12 \le h \le 11, -15 \le k \le 15, -26 \le l \le 29$
Total reflections	3832	6568
Unique reflections (R_{int})	2395 (0.0682)	2691(0.0356)
Refinement method	full-matrix least squares on F^2	full-matrix least squares on F^2
Data/restraints/parameters	3832/2/215	6568/15/292
Goodness-of-fit (GOF) on F^2	1.226	1.015
R factor [$I > 2\sigma(I)$]	$R_1 = 0.0830$, w$R_2 = 0.1983$	$R_1 = 0.0284$, w$R_2 = 0.0671$
R factor (all data)	$R_1 = 0.1284$, w$R_2 = 1.225$	$R_1 = 0.0912$, w$R_2 = 1.016$
Max and min residual electron density (e/$Å^3$)	1.951 and −1.274	1.897 and −2.787
Flack parameter	0.39(2)	

Absorption corrections were applied using a semi-empirical procedure [22]. Both structures were solved by direct methods and refined on F^2 by full-matrix least-square techniques using SHELXTL-2015 program package [23]. All non-hydrogen atoms were refined anisotropically. The positions of hydrogen atoms from the water molecules were assigned from the electronic density map generated by Fourier difference and they were refined freely. The DIAMOND program [24] was used to visualize the processed crystallographic data and to generate graphics. Details of the crystallographic data and structure refinement parameters for **1** and **2** are summarized in Table 1 and selected bond lengths and angles in Table 2.

3. Results and discussion

3.1. Synthesis, IR and UV–Vis spectra of *1* and *2*

An obvious efficient method for the preparation of the target salts (in 82% yield) is shown in Scheme 1. In an aqueous solution, the precursor $Ag_3[Cr(C_2O_4)_3]\cdot 3H_2O$ reacts on one hand with $SrCl_2\cdot 6H_2O$ and KCl to afford the salt $SrK_{0.5}Ag_{0.5}[Cr(C_2O_4)_3]$ (**1**) and, on the other hand, with $SrCl_2\cdot 6H_2O$ to form the salt $SrAg[Cr(C_2O_4)_3]\cdot 6H_2O$ (**2**). Crystals of these polymeric salts are stable in air at room temperature, but aging crystals exhibit a tremendous sheen at their surfaces. Elemental analysis results of the two salts are consistent with the single-crystal X-ray results.

In the IR spectrum of **1** (Fig. S1), there is practically no band in the region 3450–3400 cm^{-1}, confirming the absence of water molecules in its structure. In **2** (Fig. S2), the broad band centered at ca. 3400 cm^{-1} is attributed to the stretching vibrations of water molecules ν(O–H) [25]. In the region 1650–400 cm^{-1}, FT–IR spectra are very similar for the two salts. The characteristic bands of the carboxylate groups in **1** and **2** appear in the usual region at 1620–1639 cm^{-1} for the antisymmetric stretching vibrations and at 1380–1416 cm^{-1} for the symmetric stretching vibrations, respectively [26]. In **1**, a medium band centered at ca. 853 cm^{-1}, which is absent in **2**, is assigned to ν(K–O) [27]. Other bands centered at ca. 543 cm^{-1}, 470 cm^{-1} (474 cm^{-1} for **1**, 476 cm^{-1} for **2**) and 409 cm^{-1} are ascribed to ν(Cr–O), ν(Sr–O) and ν(Ag–O), respectively [28].

The UV–Vis spectra of **1** (Fig. S3) and **2** (Fig. S4) exhibit similar profiles characterized by two absorption bands, the peaks of which lie around 418 and 569 nm for **1**, and 420 and 571 nm for **2**. These absorptions are compatible with *d-d* electronic transitions within the octahedral complex ion $[Cr(C_2O_4)_3]^{3-}$ contained in **1** and **2** [29–31].

3.2. Structure descriptions

3.2.1. Structure description of *1*

Salt **1** crystallizes in the orthorhombic polar space group *Fdd2*. This space group is in contrast to the usual space group *C2/c* that

Table 2
Selected bond lengths (Å) and angles (°) within the coordination spheres around the metal centers in **1** and **2**.

Compound 1			
Cr1–O11^{x}	1.952(9)	O11^{x}–Cr1–O33	92.7(4)
Cr1–O33	1.966(10)	O33–Cr1–O22^{xi}	90.4(4)
Cr1–O34	1.972(10)	O33–Cr1–O34	82.4(4)
Cr1–O21^{xi}	1.978(10)	O11^{x}–Cr1–O21^{xi}	92.2(5)
Cr1–O22^{xi}	1.979(10)	O11^{x}–Cr1–O22^{xi}	92.6(4)
Cr1–O12^{xii}	1.981(10)	O22^{xi}–Cr1–O12^{xii}	172.2(4)
Sr1–O23	2.632(10)	O23–Sr1–O31	70.1(4)
Sr1–O31	2.640(12)	O31–Sr1–O24	68.8(3)
Sr1–O14	2.641(11)	O14–Sr1–O13	73.0(3)
Sr1–O24	2.667(9)	O14–Sr1–O24	70.9(3)
Sr1–O13	2.672(10)	O13–Sr1–O32	62.4(3)
Sr1–O32	2.726(9)	O23–Sr1–O32	120.9(3)
K1–O21	2.792(10)	O21–K1–O24	44.3(3)
K1–O24	3.019(10)	O21–K1–O24^{v}	120.1(3)
Ag1A–O11	2.77(3)	O11–Ag1A–O31	110.2(3)
Ag1A–O14	2.90(3)	O14–Ag1A–O11	46.4(3)
Ag1A–O31	2.96(3)	O34–Ag1A–O31	45.4(3)
Ag1A–O34	2.82(3)	O14–Ag1A–O34	103.4(3)
Ag1B–O14	2.96(3)	O14–Ag1B–O34	101.6(7)
Ag1C–O11	2.71(3)	O11–Ag1C–O31	115.5(8)
Compound **2**			
Cr1–O32	1.964(3)	O32–Cr1–O14	90.54(13)
Cr1–O14	1.965(3)	O14–Cr1–O22	95.17(13)
Cr1–O22	1.968(3)	O32–Cr1–O22	91.53(13)
Cr1–O13	1.975(3)	O13–Cr1–O31	91.41(13)
Cr1–O21	1.979(3)	O21–Cr1–O31	95.65(13)
Cr1–O31	1.985(3)	O22–Cr1–O31	91.09(14)
Ag1–O4W	2.300(4)	O4W–Ag1–O1W	109.14(18)
Ag1–O5W	2.330(4)	O4W–Ag1–O5W	157.11(18)
Ag1–O1W	2.555(6)	O5W–Ag1–O1W	89.50(16)
Sr1–O3W	2.571(4)	O3W–Sr1–C21^{ii}	82.35(12)
Sr1–O2W	2.600(3)	O3W–Sr1–O2W	70.63(13)
Sr1–O34^{i}	2.638(3)	O3W–Sr1–O34^{i}	83.15(13)
Sr1–O24^{ii}	2.646(3)	O3W–Sr1–O24^{ii}	68.06(12)
Sr1–O11^{iii}	2.646(3)	O2W–Sr1–O11^{iii}	76.46(10)
Sr1–O33^{i}	2.647(3)	O11^{iii}–Sr1–O33^{i}	77.02(10)
Sr1–O12	2.687(3)	O3W–Sr1–O12	71.17(13)
Sr1–O11	2.692(3)	O11^{iii}–Sr1–O11	63.11(11)
Sr1–O23^{ii}	2.756(3)	O34^{i}–Sr1–O23^{ii}	67.29(11)

Symmetry transformations used to generate equivalent atoms: (ii) -x, -y, z; (x) x, y, 1+z;; (v) -x, 1-y, z; (xi) -x, 1/2-y, 1/2+z; (xii) 1/4-x, −1/4+y, 3/4+z for **1** and (i) 1-x, −1/2+y, 1/2-z.
(ii) x, −1+y, z; (iii) 1-x, 1-y, -z for **2**.

a)

$$Ag_3[Cr(C_2O_4)_3]\cdot 3H_2O + SrCl_2\cdot 6H_2O + 1/2\ KCl \xrightarrow{H_2O/25°C} SrK_{0.5}Ag_{0.5}[Cr(C_2O_4)_3]\ (\mathbf{1}) + 5/2\ AgCl + 9\ H_2O$$

b)

$$Ag_3[Cr(C_2O_4)_3]\cdot 3H_2O + SrCl_2\cdot 6H_2O \xrightarrow{H_2O/25°C} SrAg[Cr(C_2O_4)_3]\cdot 6H_2O\ (\mathbf{2}) + 2\ AgCl + 3\ H_2O$$

Scheme 1. Synthetic procedure of the target salts **1** *(a)* and **2** *(b)*.

occurs for most of open-framework silver-deficient oxalatochromate(III) salts [15,17–20]. The asymmetric unit of **1** contains one $[Cr(C_2O_4)_3]^{3-}$ complex anion, one Sr^{2+} cation, one half Ag^{+} cation (disordered) and one half K^{+} cation (special position). The coordination polyhedra around the different metallic centers are highlighted in Fig. 1. The central Cr^{3+} ion of the complex anion (Fig. 1a) is coordinated by six O atoms (O11, O12, O21, O22, O33, O34) from three chelating oxalato(2−) ligands in a slightly distorted (2 + 2 + 2) octahedral coordination sphere. The structural parameters (Table 2) within the $[Cr(C_2O_4)_3]^{3-}$ ions with respect to their geometry, bond lengths and bond angles, are similar to those found in salt **2**.

Each Sr1 site (Fig. 1b) is eight-coordinate, being linked in a monodentate manner to eight oxygen atoms (O13, O13', O14, O23, O24, O31, O32, O32') of oxalate ligands. Two neighboring Sr^{2+} form a pseudo-dimer. This dimer with its two Sr sites can be visualized adequately as the association of two non-identical, asymmetric monomers, the reason it is dubbed "pseudo-dimeric". Sr–O bond lengths range from 2.632(10) to 2.726(9) Å and the O–Sr–O angles from 62.8(3) to 134.5(3) °. The Ag atom (Fig. 1c) is in tetra-coordination of oxalato-O atoms (O11, O14, O31, O34) with Ag–O bond lengths ranging from 2.71 (3) to 2.96(3) Å. Ag is highly disordered over four sites, three of which (Ag1A, Ag1B and Ag1C) are very close to each other with occupancies of 0.210(3), 0.076(4)

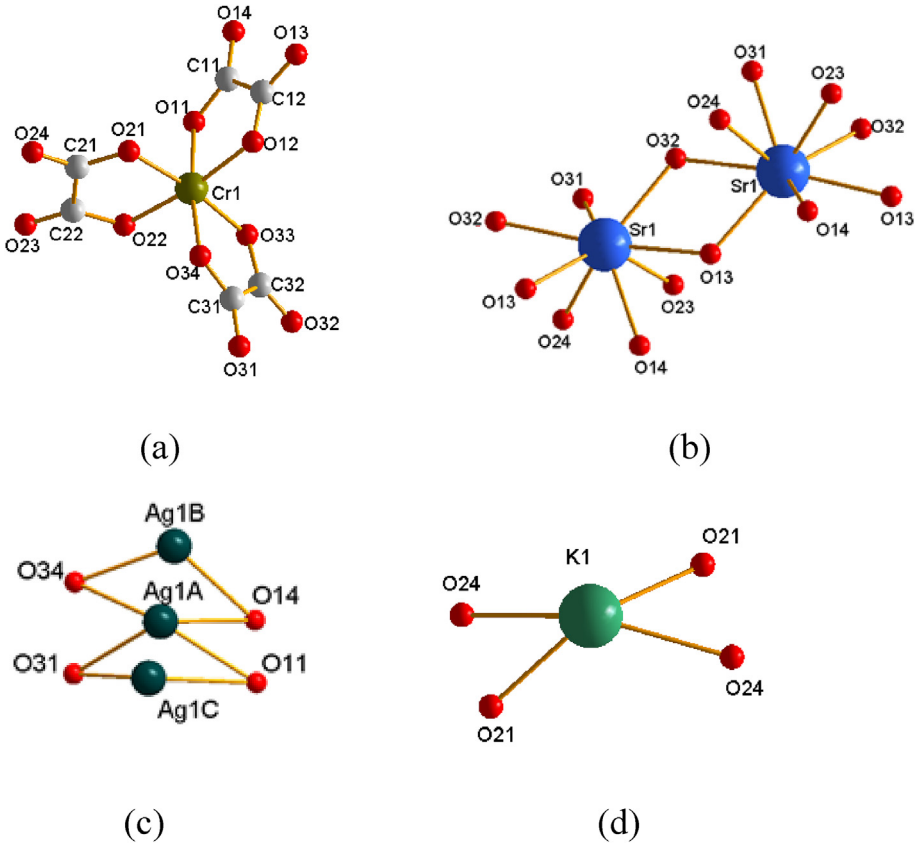

Fig. 1. Coordination environment of a) Cr^{3+}, b) Sr^{2+}, c) Ag^{+} and d) K^{+} ions in **1** with the atom numbering scheme.

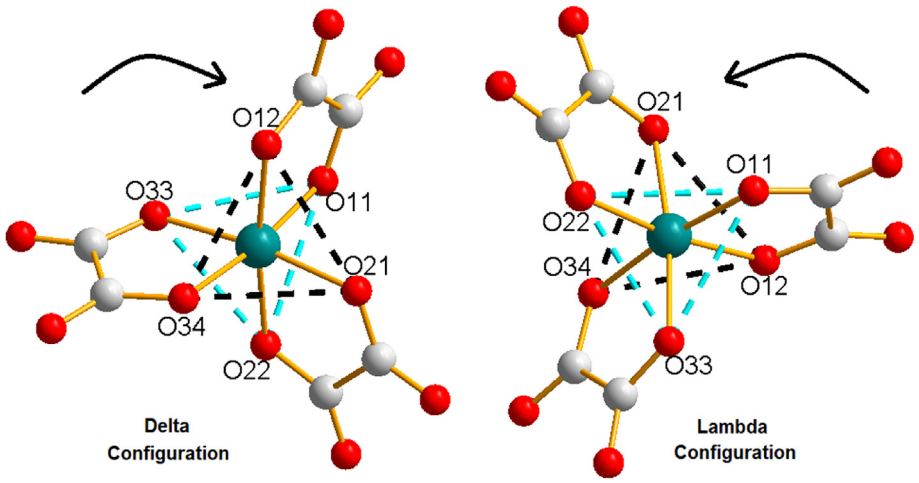

Fig. 2. The delta- and lambda-configurations of metal oxalates in the unit cell of **1**.

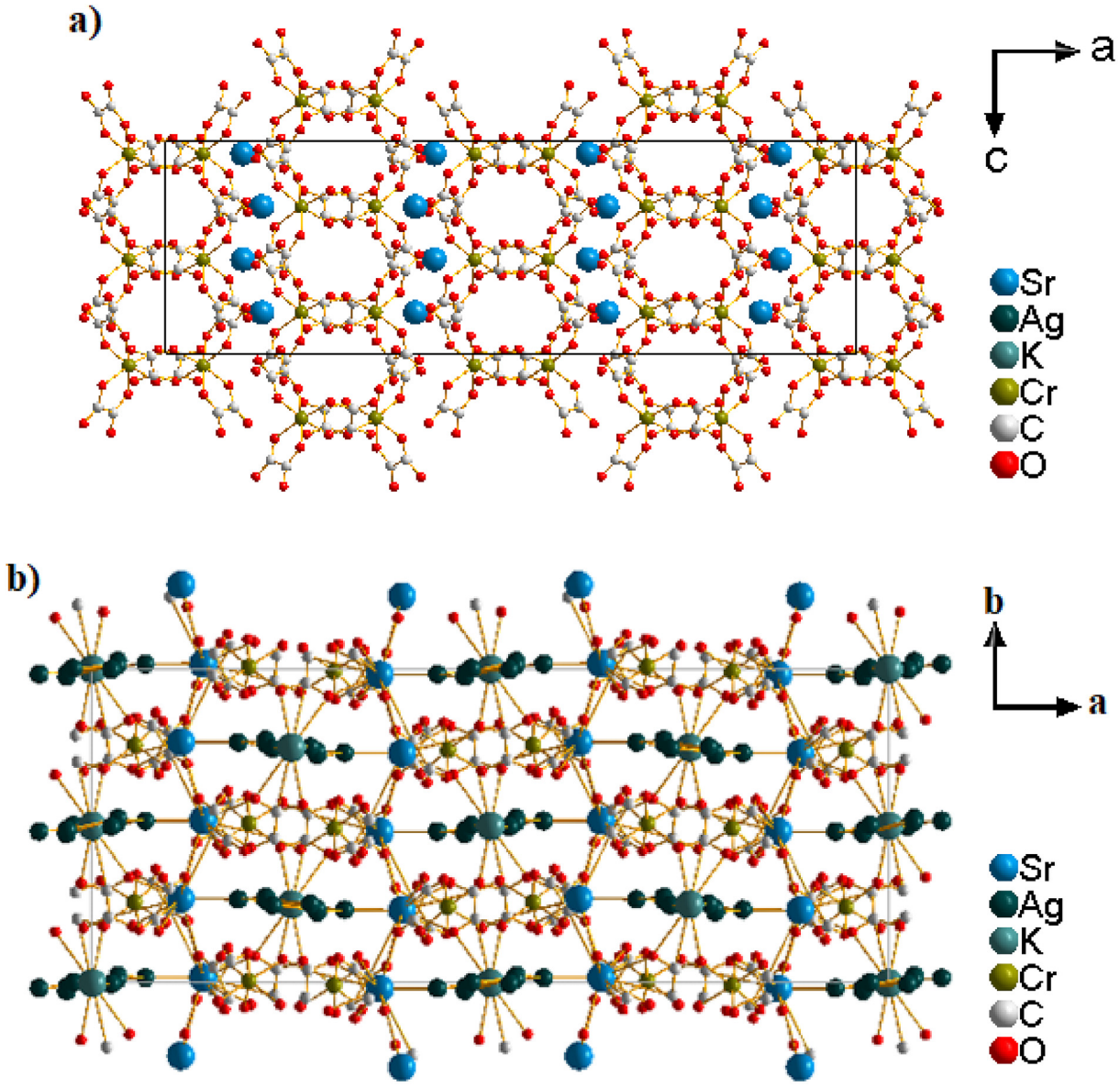

Fig. 3. a) Packing diagram of **1** showing nanochannels parallel to b axis. Sr^{2+} ions are in between nanochannels; b) the 3-dimensional interconnectivity between $[Cr(C_2O_4)_3]^{3-}$ complex anions, Ag^{+}, K^{+} and Sr^{2+} cations.

and 0.069(3) while the fourth (Ag2) sits at a farther position and has an occupancy of 0.146(4). The sum of all Ag occupancies matches the occupancy of K (special position 0, thereby accounting for the overall neutrality of the compound. The K atom (Fig. 1d) is tetracoordinated by oxalato-O atoms (O21, O21′, O24, O24') with bond distances K1−O21 = 2.792(10) Å and K1−O21 = 3.019(10) Å. Fig. 2 shows the delta- and lambda-configurations of metal oxalates in the unit cell of salt **1**.

A packing diagram of **1** is depicted in Fig. 3. The anionic framework built exclusively from the tris(oxalato)chromate(III) complex anions, $[Cr(C_2O_4)_3]^{3-}$, forms nanochannels (ca 6.7 Å) parallel to *b* axis (Fig. 3a). This anionic grid is counter-balanced by K^+ and Ag^+ cations located inside the channels and by Sr^{2+} cations located in between walls of neighboring channels. The 3-dimensional interconnectivity between $[Cr(C_2O_4)_3]^{3-}$ complex anions, Ag^+, K^+ and Sr^{2+} cations is highlighted in Fig. 3b. Salt **1** exhibits the highest value of silver-deficiency (x = 2.5) known so far for open-framework silver-deficient oxalatochromate(III) salts [15–20].

3.2.2. *Structure description of* **2**

Salt **2** crystallizes in the monoclinic system with space group $P2_1/c$. The asymmetric unit of **2** contains one tris(oxalato)chromate(III) complex anion, $[Cr(C_2O_4)_3]^{3-}$, one Ag^+ cation, one Sr^{2+} cation and six water molecules. The environment of the metallic centers in **2** is illustrated in Fig. 4. The central Cr^{3+} ion of the complex anion (Fig. 4a) is coordinated by six O atoms (O13, O14, O21, O22, O31, O32) from three chelating oxalato(2−) ligands in a slightly distorted (2 + 2 + 2) octahedral coordination sphere. The Cr−O bond lengths range from 1.964(3) to 1.985(3) Å and the O−Cr−O angles, from 90.54(13) to 95.65(13) ° (Table 2). These geometric parameters are very similar to those reported previously in salts involving the tris(oxalato)chromate(III) complex anions, $[Cr(C_2O_4)_3]^{3-}$ [32–34]. Each Sr1 site (Fig. 4b) is nine-coordinate, being linked in a monodentate manner to seven oxygen atoms (O11, $O11^i$, O12, O23, O24, O33, O34) of oxalate ligands and two oxygen atoms (O2W, O3W) of water molecules. Two neighboring Sr1 sites form a $[Sr_2O_{18}]$ unit with inversion symmetry. The Sr−O bond lengths range from 2.571(4) to 2.692(3) Å, and the O−Sr−O angles, from 63.11(11) to 83.15(13) ° (Table 2). The Ag site (Fig. 4c) exhibits a three-coordinate mode of O atoms (O1W, O4W, O5W) to water molecules with different bond distances Ag1−O4W = 2.300(4), Ag1−O5W = 2.330(4) and Ag1−O1W = 2.555(6) Å.

The packing diagram of **2** is illustrated in Fig. 5. Salt **2** can be best described as a non-molecular coordination polymer where the 3-D unit cell framework is realized by the chemical interconnection of the metallic centers (Cr, Sr and Ag) through the O atoms of the oxalates and water molecules. The resulting rigid "skeleton" (Fig. 5a) delineates elliptic channels that extend parallel to *b* axis, hosting crystal water molecules. Two types of H_2O-guest molecules are distinguishable inside the channels: those coordinated to the metallic centers Sr (O2W, O3W) and Ag (O1W, O4W, O5W) and the O6W which actually represents the only crystal water in the formula unit of salt **2**. Compared to the well-known salt $Ag_3[Cr(C_2O_4)_3]\cdot 3H_2O$ [15] with no silver-deficiency, salt **2** can be seen as a nanochanneled silver-deficient oxalatochromate(III) coordination polymer with a silver deficiency value x = 2.

Hydrogen bond lengths (Å) and bond angles (°) in **2** are shown in Table 3. The bulk structure (Fig. 5b) is consolidated by a network of hydrogen bonds of the type O−H···O [2.734(5) to 3.142(5) Å] linking water molecules and the surrounding oxalate O atoms.

Host lattice networks and silver-deficit values for some nanochanneled Ag(I)/Cr(III) oxalate coordination polymers are listed in Table 4. They confirm that silver-deficiencies values (x ≥ 2) found in compounds **1** and **2** are the highest obtained so far for this family of salts. Interestingly, crystals of **1** and **2** exhibit a tremendous metallic sheen at their surfaces, suggesting formation of a superficial metallic layer, much likely due to the reduction of the most external Ag^+ ions. This observation lends good grounds to suspect considerable electrical conductivity in such crystals. This is an important result which is worth following up in future research.

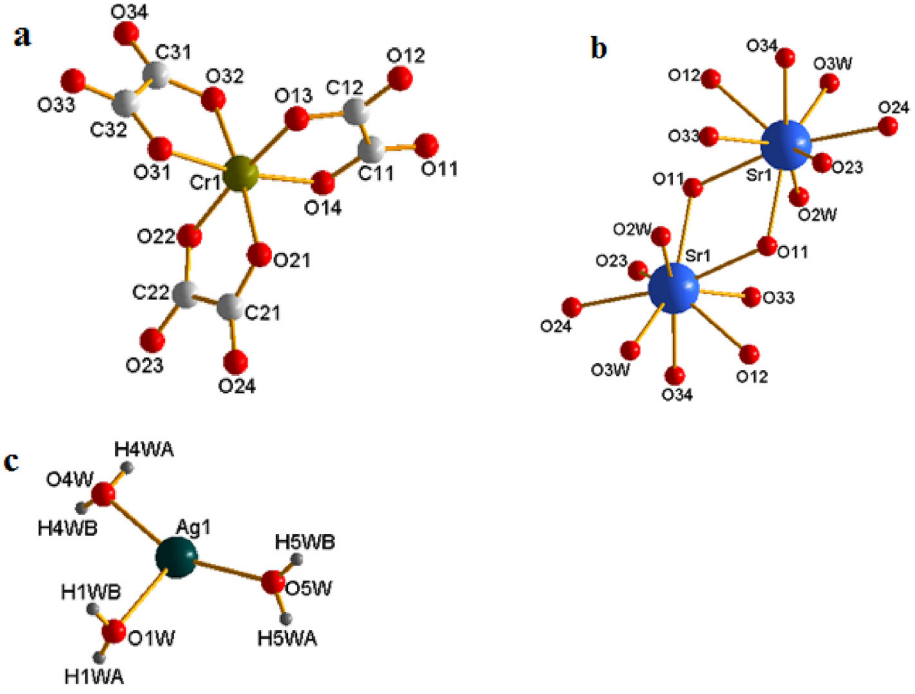

Fig. 4. Coordination environment of a) Cr^{3+}, b) Sr^{2+} and c) Ag^+ ions in **2** with the atom numbering scheme.

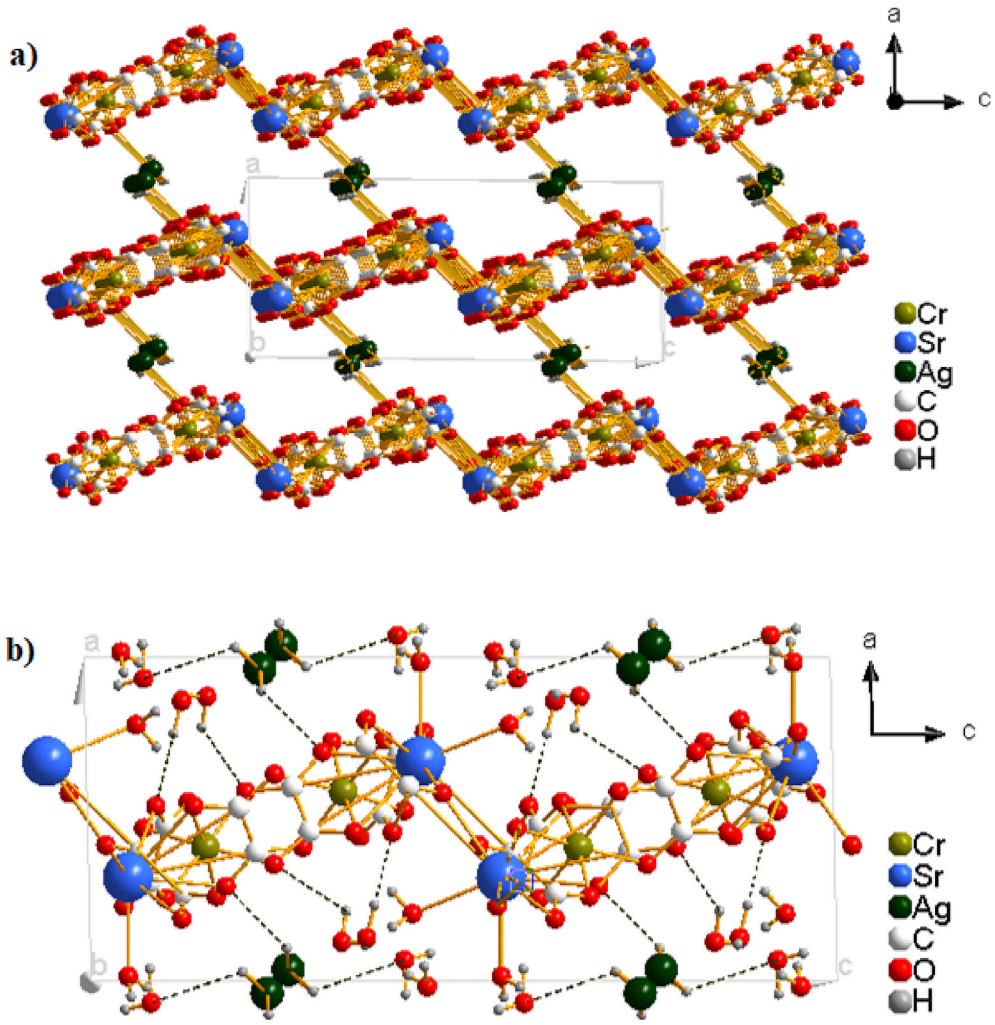

Fig. 5. Packing diagram of **2** highlighting a) nanochannels parallel to b axis and b) O–H···O hydrogen bonding interactions (dashed lines).

Table 3
Hydrogen bond lengths (Å) and bond angles (°) in **2**.

D–H … A	d(D–H)	d(H … A)	d(D … A)	< (DHA)
O1W–H1WA … O31	0.75(7)	2.24(7)	2.912(6)	149
O1W–H1WB···O12^{i}	0.74(7)	2.25(7)	2.975(6)	167
O2W–H2WA … O5W^{ii}	0.79(4)	2.03(5)	2.800(5)	165
O2W–H2WB···O33^{iii}	0.88(5)	1.92(6)	2.784(4)	167
O3W–H3WA … O2W^{ii}	0.81(4)	2.11(4)	2.912(6)	176
O3W–H3WB···O4W^{iv}	0.80(4)	2.05(7)	2.842(6)	171
O4W–H4WA … O6W^{v}	0.78(7)	2.20(7)	2.901(7)	150
O4W–H4WB···O22^{vi}	0.87(8)	2.51(9)	3.142(5)	130
O4W–H4WB···O23^{vi}	0.87(8)	1.95(7)	2.816(5)	171
O5W–H5WA … O6W^{vii}	0.86(5)	1.94(3)	2.737(7)	155
O5W–H5WB···O32^{ix}	0.84(4)	2.21(10)	2.734(5)	121
O6W–H6WA … O21^{vii}	0.89(4)	1.88(11)	2.753(5)	166
O6W–H6WB···O24^{viii}	0.73(5)	2.18(11)	2.882(6)	159

Symmetry transformations used to generate equivalent atoms (D, donor; A, acceptor).
(i) -x, 1/2+y, 1/2-z; (ii) -x, 1-y, -z; (iii) x, 3/2-y, −1/2+z; (iv) -x, −1/2+y, 1/2-z; (v) x, 1/2-y.
−1/2+z; (vi) 1-x, −1/2+y, 1/2-z; (vii) -x, 1-y, 1-z; (viii) x, −1+y, 1+z; (ix) −1+x, y, z.

3.3. Powder XRD and thermal behavior of *1* and *2*

To check the phase purity of salts **1** and **2**, powder X-ray diffraction (PXRD) was carried out at room temperature. As shown in Fig. S5, for **2**, the PXRD pattern matches well with the simulated pattern, confirming bulk phase purity. However, for **1** the pattern does not match that simulated from the single crystal structure. This could be because the crystals aged in the diffractometer due to heat inside the instrument.

The thermal behavior of salts **1** and **2** was examined by thermogravimetric analysis (TGA) and differential scanning calorimetry (DSC) in an air atmosphere with a heating rate of 10 °C·min^{-1} in the temperature range of 25–700 °C (Fig. 6). There is no apparent mass loss up to 250 °C in the TGA curve (Fig. 6a) of compound **1**, confirming the absence of crystal waters in its structure. The decomposition of the framework which is associated with an exothermic effect, finally occurs between 250 and 450 °C with release of 6 CO_2, leading to 55.4% mass loss (calcd. 55.1%). For compound **2**, the TGA curve (Fig. 6b) presents two major mass losses: the first endothermic mass loss of 9.0% (calcd. 8.8%) occurs from room temperature up to around 90 °C and corresponds to the release of three water molecules. The decomposition of the framework which is associated with an exothermic effect, occurs between 250 and 320 °C with release of (3 CO_2 + 3H_2O) leading to 31.9% mass loss (calcd. 31.6%).

3.4. Magnetic properties

EPR spectra for both compounds (Fig. 7) were measured at room temperature. The spectrum of **1** displays an anisotropy of g factor

Table 4
Selected host lattice networks, silver deficits and space groups for nanochanneled Ag(I)/Cr(III) oxalate coordination polymers.

Compound	Host lattice network	Charge balance	Silver deficit	Space group	Ref.
$Ag_3[Cr(ox)_3]\cdot 3H_2O$	$[Ag_3Cr(ox)_3]^{0.00}$	0.00	0.00	C_2/c	[15]
$H_{0.10}[Ag_{2.90}Cr(ox)_3]\cdot 3.75H_2O$	$[Ag_{2.90}Cr(ox)_3]^{0.10-}$	$H^+_{0.1}$	0.10	$P2_1/n$	[16]
$Cs_{0.19}[Ag_{2.81}Cr(ox)_3]\cdot 3H_2O$	$[Ag_{2.81}Cr(ox)_3]^{0.19-}$	$Cs^+_{0.19}$	0.19	C_2/c	[15]
$K_{0.24}[Ag_{2.76}Cr(ox)_3]\cdot 3H_2O$	$[Ag_{2.76}Cr(ox)_3]^{0.24-}$	$K^+_{0.24}$	0.24	C_2/c	[18]
$K_{0.28}[Ag_{2.72}Cr(ox)_3]\cdot 3H_2O$	$[Ag_{2.72}Cr(ox)_3]^{0.28-}$	$K^+_{0.28}$	0.28	C_2/c	[15]
$Cs_{0.41}[Ag_{2.50}Cr(ox)_3]\cdot 3H_2O$	$[Ag_{2.59}Cr(ox)_3]^{0.41-}$	$Cs^+_{0.41}$	0.41	C_2/c	[15]
$Cs_{0.43}[Ag_{2.57}Cr(ox)_3]\cdot 3H_2O$	$[Ag_{2.57}Cr(ox)_3]^{0.43-}$	$Cs^+_{0.43}$	0.43	C_2/c	[15]
$H_{0.50}[Ag_{2.50}Cr(ox)_3]\cdot 5H_2O$	$[Ag_{2.50}Cr(ox)_3]^{0.50-}$	$H^+_{0.50}$	0.50	C_2/c	[17]
$Cr_{0.25}[Ag_{2.25}Cr(ox)_3]\cdot 5H_2O$	$[Ag_{2.25}Cr(ox)_3]^{0.75-}$	$Cr^{3+}_{0.25}$	0.75	C_2/c	[20]
$Ba_{0.50}[Ag_2Cr(ox)_3]\cdot 5H_2O$	$[Ag_2Cr(ox)_3]^{-}$	$Ba^{2+}_{0.50}$	1.00	C_2/c	[19]
$Sr[AgCr(ox)_3]\cdot 6H_2O$	$[AgCr(ox)_3]^{2-}$	Sr^{2+}	2.00	$P2_1/c$	This work
$SrK_{0.50}[Ag_{0.5}Cr(ox)_3]$	$[Ag_{0.5}Cr(ox)_3]^{2.5-}$	Sr^{2+}; K^+	2.50	$Fdd2$	This work

ox: oxalate dianion $C_2O_4^{2-}$.

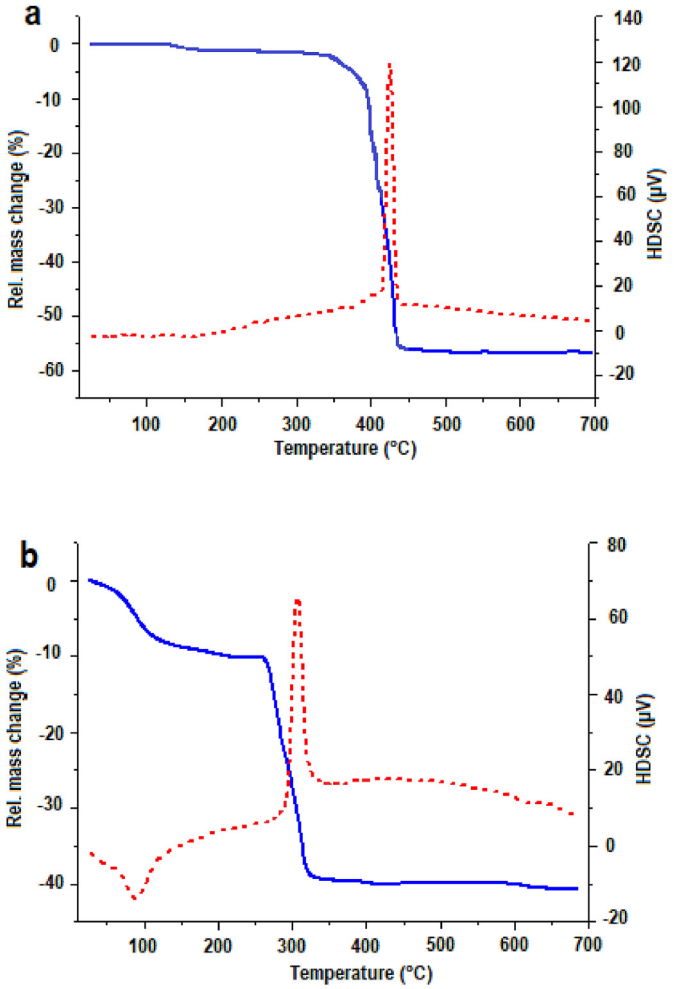

Fig. 6. TGA (blue) and DSC (red) diagrams for **1** (a) and **2** (b).

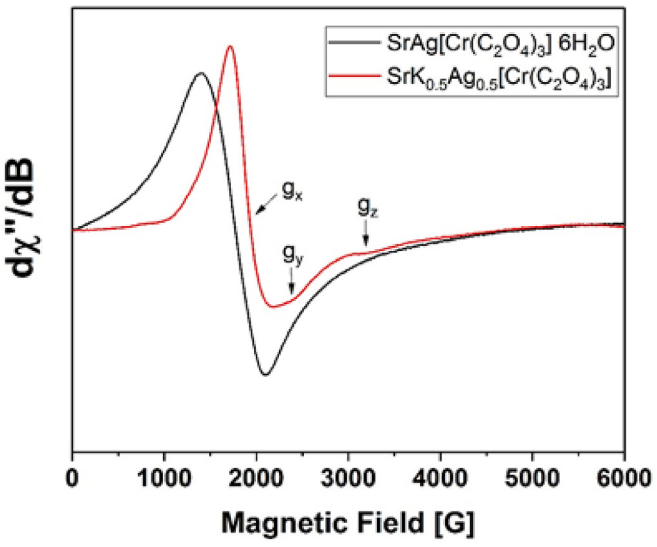

Fig. 7. Room temperature EPR spectra for **1** and **2**.

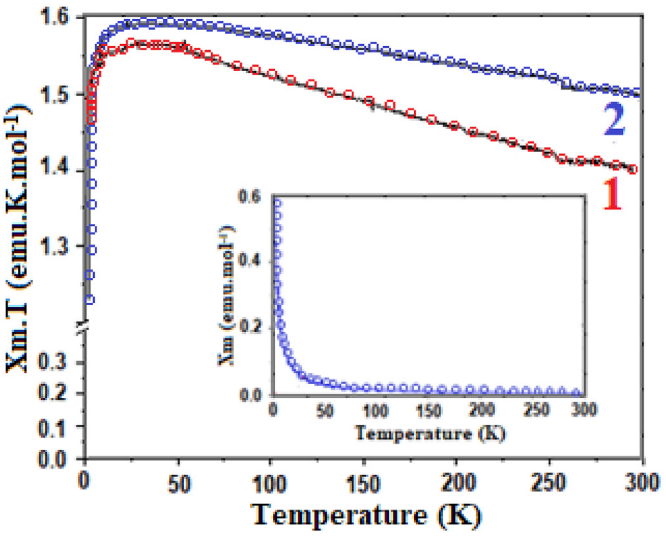

Fig. 8. Plots of the magnetic susceptibility, χM, and χMT as functions of temperature.

($g_x = 3.70$, $g_y = 3.01$ and $g_z = 2.18$) whereas for compound **2**, the spectrum shows a very broad line with a g factor of 4.01. These spectra are typically characteristic of high spin S = 3/2 Cr(III) complexes. For compound **1**, the g anisotropy with three different Eigen values indicates an octahedral distortion.

The direct-current (dc) magnetic properties of **1** and **2** in the form of $\chi_M T$ *vs* T plots (with χ_M being the molar magnetic susceptibility and T the temperature) are shown in Fig. 8.

The experimental data for compounds **1** and **2** show a gradual increase in the value of $\chi_M T$ with decreasing temperature to reach a

maximum at ~20 K and then decreases, indicative of weak antiferromagnetic interactions between isolated Cr^{III} centers in the two compounds at low temperatures [35]. The magnetic exchange pathway takes place through oxalato-bridged Cr^{III} units, the chromium-chromium spacings being 6.75 Å and 6.71 Å for **1** and **2**, respectively.

4. Conclusion

Two nanochanneled silver-deficient coordination polymers, $SrK_{0.5}Ag_{0.5}[Cr(C_2O_4)_3]$ (**1**) and $SrAg[Cr(C_2O_4)_3]\cdot 6H_2O$ (**2**) have been synthesized and structurally, as well as magnetically characterized. The observation of higher silver-deficiencies ($x \geq 2$) in this family of polymerized oxalatochromate(III) salts is unprecedented. XRD results confirmed the formation of a single phase of each synthesized salt. Magnetic susceptibility measurements revealed weak antiferromagnetic interactions between Cr(III) ions in **1** and **2**.

These findings not only expand the family of nanochanneled silver-deficient oxalatochromate(III) coordination polymers, but also further demonstrate the highly flexible and promising route to vary substantially the host framework $[Ag_{3-x}Cr(C_2O_4)_3]^{x-}$ from one system to the other. Furthermore, the results of this work suggest that the family of materials with variable Ag–Cr-oxalate channel frameworks may be extended to the Ag-M^{III}-oxalate series, where M^{III} = Al, Fe, Ru, Rh, etc. The realization of this objective now stands as a priority on the agenda of our forthcoming research.

It is worth noting finally, that crystals of **1** and **2** exhibit a tremendous metallic sheen at their surfaces, suggesting formation of a superficial metallic layer, much likely due to the reduction of the most external Ag^+ ions. This observation lends good grounds to suspect considerable electrical conductivity in such crystals which, indeed, adds some more value to the research and development of this category of materials.

Declaration of competing interest

The authors declare that they have no known competing financial interests or personal relationships that could have appeared to influence the work reported in this paper.

Acknowledgements

This work was partially supported by the National Science Foundation Career Award to BPTF (no. DMR-1654780).

Appendix A. Supplementary data

Supplementary data to this article can be found online at https://doi.org/10.1016/j.molstruc.2020.128642.

References

[1] S.R. Battern, R. Robson, Angew. Chem. Int. Ed. 37 (1998) 1460.
[2] R. Robson, J. Chem. Soc., Dalton Trans. (2000) 3735.
[3] M. Kondo, T. Okubo, A. Asami, S. Noro, T. Yoshitomi, S. Kitagawa, T. Ishii, H. Matsuzaka, K. Seki, Angew. Chem. Int. Ed. 43 (2004) 140.
[4] H.L. Li, M. Eddaoudi, M. O'keeffe, O.M. Yaghi, Nature 402 (1999) 276.
[5] J.Y. Lee, O.K. Farha, J. Roberts, K.A. Scheidt, S.T. Nguyen, J.T. Hupp, Chem. Soc. Rev. 38 (2009) 1450.
[6] K. Ohara, M. Kawano, Y. Inokuma, M. Fujita, J. Am. Chem. Soc. 132 (2010) 30.
[7] M.X. Yao, Q. Zheng, X.M. Cai, Y.Z. Li, Y. Song, J.L. Zuo, Inorg. Chem. 51 (2012) 2140.
[8] Q. Liu, L.L. Yu, Y. Wang, Y.Z. Ji, J. Horvat, M.L. Cheng, X.Y. Jia, G.X. Wang, Inorg. Chem. 52 (2013) 2817.
[9] O.R. Evans, R. Xiong, R. Wang, G.K. Wong, W. Lin, Angew. Chem. Int. Ed. 38 (1999) 536.
[10] B.J. Coe, S.P. Foxon, E.C. Harper, M. Helliwell, J. Raftery, C.A. Swanson, B.S. Brunschwig, K. Clays, E. Franz, J. Garin, J. Orduna, P.N. Horton, M.B. Hursthouse, J. Am. Chem. Soc. 132 (2010) 1706.
[11] N.L. Rosi, J. Eckert, M. Eddaoudi, D.T. Vodak, J. Kim, M. O'Keeffe, O.M. Yaghi, Science 300 (2003) 1127.
[12] B. Kesanli, Y. Cui, M.R. Smith, E.W. Bittner, B.C. Bockrath, W. Lin, Angew. Chem. Int. Ed. 44 (2005) 72.
[13] P.K. Thallapally, J. Tian, M.R. Kishan, C.A. Fernandez, S.J. Dalgarno, P.B. McGrail, J.E. Warren, J.L. Atwood, J. Am. Chem. Soc. 130 (2008) 16842.
[14] E.C. Constable, Aust. J. Chem. 59 (2006) 1.
[15] P.A.W. Dean, D. Craig, I. Dance, V. Russell, M. Scudder, Inorg. Chem. 43 (2004) 443.
[16] M.M. Bélombé, J. Nenwa, Y.A. Mbiangué, G. Bebga, F. Majoumo-Mbé, E. Hey-Hawkins, P. Lönnecke, Inorg. Chim. Acta. 362 (2009) 1.
[17] C.T. Eboga, G. Bebga, Y.A. Mbiangué, E.N. Nfor, P.L. Djonwouo, M.M. Bélombé, J. Nenwa, Open J. Inorg. Chem. 7 (2017) 75.
[18] G. Bebga, M. Signé, J. Nenwa, B.P.T. Fokwa, Res. J. Chem. Environ. 17 (2013) 57.
[19] C.T. Eboga, B.N. Ndosiri, Y.A. Mbiangué, G. Bebga, J. Nenwa, Am. J. Anal. Chem. 7 (2016) 99.
[20] M.M. Bélombé, J. Nenwa, O.T. Tene, B.P.T. Fokwa, Glob. J. Inorg. Chem. 1 (2010) 34.
[21] A. Earnshaw, Introduction to Magnetochemistry, Academic Press, London, 1968.
[22] G.M. Sheldrick, SADABS, University of Göttingen, Göttingen, Germany, 2010.
[23] G.M. Sheldrick, Acta Crystallogr. C71 (2015) 3.
[24] G.M. Sheldrick, Acta Crystallogr. A64 (2008) 112.
[25] Z. Xiong, P. Yuan, Z. Xie, G. Li, Supramol. Chem. 26 (2014) 346.
[26] F. Zhang, Z. Li, T. Ge, H. Yao, G. Li, H. Lu, Y. Zhu, Inorg. Chem. 49 (2010) 3776.
[27] K. Nakamoto, Infrared Spectra of Inorganic and Coordination Compounds, Wiley-Interscience, New York, 1970.
[28] L.J. Bellamy, Infrared Spectra of Complex Molecules, Chapman and Hall, New York, 1980.
[29] M.M. Bélombé, J. Nenwa, Y.A. Mbiangué, G.E. Nnanga, I.M. Mbomékallé, E. Hey-Hawkins, P. Lönnecke, F. Majoumo-Mbé, Dalton Trans. (2003) 2117.
[30] S. Decurtins, H.W. Schmalle, H.R. Oswald, A. Linden, J. Ensling, P. Gütlich, A. Hauser, Inorg. Chim. Acta. 216 (1994) 65.
[31] A. Roy, K. Nag, J. Inorg. Nucl. Chem. 40 (1978) 1501.
[32] S. Decurtins, M. Gross, H.W. Schmalle, S. Ferlay, Inorg. Chem. 37 (1998) 2443.
[33] M.M. Bélombé, J. Nenwa, Y.A. Mbiangué, F. Majoumo-Mbé, P. Lönnecke, E. Hey-Hawkins, Dalton Trans. (2009) 4519.
[34] N.M.M. Houga, F. Capet, J. Nenwa, G. Bebga, M. Foulon, Acta Crystallogr. E71 (2015) 1408.
[35] R. Dridi, C. Dhieb, S.N. Cherni, N.C. Boudjaka, N.S. Zouaoui, M.F. Zid, J. Mol. Struct. 1152 (2018) 294.